LC-DET-2012-081

Conceptual Design of the ILD Detector Magnet System

F.Kircher[1)], O. Delferriere[1)], L. Scola[1)], M. Lemke[2)], A. Petrov[2)], K. Sinram[2)], U. Schneekloth[2)], R. Stromhagen[2)], B. Curé[3)], K. Elsener[3)]

[1)] CEA, Paris, France
[2)] DESY, Hamburg, Germany
[3)] CERN, Geneva, Switzerland

Abstract

This note describes the conceptual design of the ILD magnet system, which consists of a very large superconducting solenoid, its iron yoke, and an anti-DID (Detector Integrated Dipole), the aim of which is to reduce pair background hits in the very forward detectors. The design parameters of this magnet are to produce a central field of up to 4 T, in a volume of about 275 m^3 (useful diameter 6.88 m over a length of 7.35 m). A description of the ancillary systems is also included in this report.

11 June 2013

Table of contents

1 Introduction

The International Large Detector (ILD, [1]) is a concept for a detector at the International Linear Collider (ILC). This concept is based on the earlier GLD and LDC detector concepts, which joined forces in 2007 to form the ILD concept group. This note describes some details of the ILD magnet system conceptual design, beyond the summary given in the ILD DBD [1].

The design of the ILD concept is driven by the requirement to enable precision measurements, through excellent calorimetry and tracking. The whole system of calorimeters is immersed in a strong magnetic field. In addition, the iron yoke is instrumented to not only return the magnetic flux of the solenoid, but also to serve as a muon filter, muon detector and tail catcher.

As the interaction region of the ILC is designed to host two detectors, which can be moved in and out of the beam position with a push-pull scheme, the ILD overall system has been designed to be, in terms of stray field and radiation safety, as hermetic as possible.

Finally, an anti-DID (Detector-Integrated-Dipole) has been included in the ILD magnetic system. This dipole field will steer a maximum of e^+e^- pairs from beam-beam interactions towards exit holes in the very forward calorimeters. In this way, both the background rates in these calorimeters as well as the rate of backscattered particles, hitting e.g. the vertex detector, are minimized.

2 Magnetic field requirements for physics

The basic layout of the ILD detector has followed the strategy of tracking in a magnetic field. The large detector version (lower field in a larger volume) was found to have a better overall performance than the smaller one (higher field in a lower volume) [2]. Consequently the ILD detector design asks for a 3.5T and maximum 4 T central field in a warm aperture of 6.88 m in diameter and 7.35 m length. Because of the presence of an anti-DID (Detector-Integrated-Dipole), with a 0.035 T maximum dipolar field, no stringent field homogeneity is requested, despite the presence of the TPC as main tracking detector [3]. Instead, an accurate field mapping will be requested before installation of the sub-detectors inside the solenoid. For safety reasons, constraints have been put on the fringe field: less than 50 G @ R = 15 m from the IP in the radial direction.

The iron yoke, besides shielding the magnetic field, will be instrumented to be used for the detection of muons and for measuring showers escaping the HCAL (tail catcher). In addition, the yoke serves as the main mechanical structure of the ILD detector and, combined with the calorimeter, should be self-shielding in terms of radiation protection.

3 Magnet general design

The ILD magnet design is very similar to the one of CMS [4], except for its geometrical dimensions, and the presence of the anti-DID. Consequently, many technical solutions successfully used for CMS are proposed for the design of the ILD magnet.

The magnet consists of three parts:
- the superconducting solenoid coil, made of 3 modules, mechanically and electrically connected. With its thermal shields, it makes up the cold mass, supported inside the vacuum tank by several sets of tie-rods.
- the anti-DID, located on the outer radius of the main solenoid but inside the same vacuum tank. The anti-DID is designed to generate a horizontal maximum dipolar field of 0.035 T @ z = 3 m from the IP
- the iron yoke, consisting of the barrel yoke (made of 3 rings) and the two end-cap yokes, of dodecagonal shape. The yokes are laminated to house muon detectors.

A schematic cross section of the magnet system is given in Fig. 1. The main geometrical parameters of the ILD magnet are summarized in Table 1.

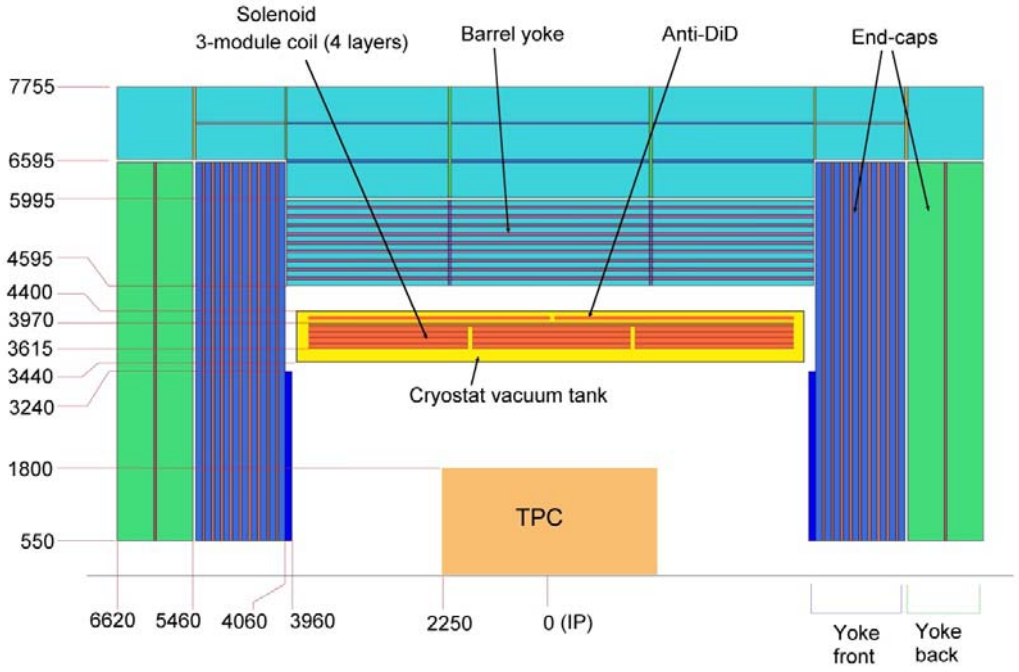

Figure 1: Schematic view of the ILD magnet cross section (to simplify the picture, only one half of the magnet section is shown).

Table1: ILD magnet main parameters

Cryostat inner radius (mm)	3440	Barrel yoke outer radius (mm)	7755
Cryostat outer radius (mm)	4400	Yoke overall length (mm)	13240
Cryostat length (mm)	7810	Barrel weight (t)	6900
Cold mass weight (t)	170	End cap weight (t)	6500
Barrel yoke inner radius (mm)	4595	Total yoke weight (t)	13400

The magnetic field map of the complete magnet system including anti-DID has been calculated in 3D, using the code Opera-3D/ TOSCA. For this calculation, the actual design of the yoke, taking into account all the gaps has been used, but using a cylindrical rather than dodecagonal geometry. Fig. 2 is a view of the meshing used. Fig. 3 shows the B-H curve for the iron in the yoke used for all the calculations. Figs. 4 and 5 show respectively the main component B_z of the field along the beam axis, and the field in various regions of the magnet for a central field of 4 T.

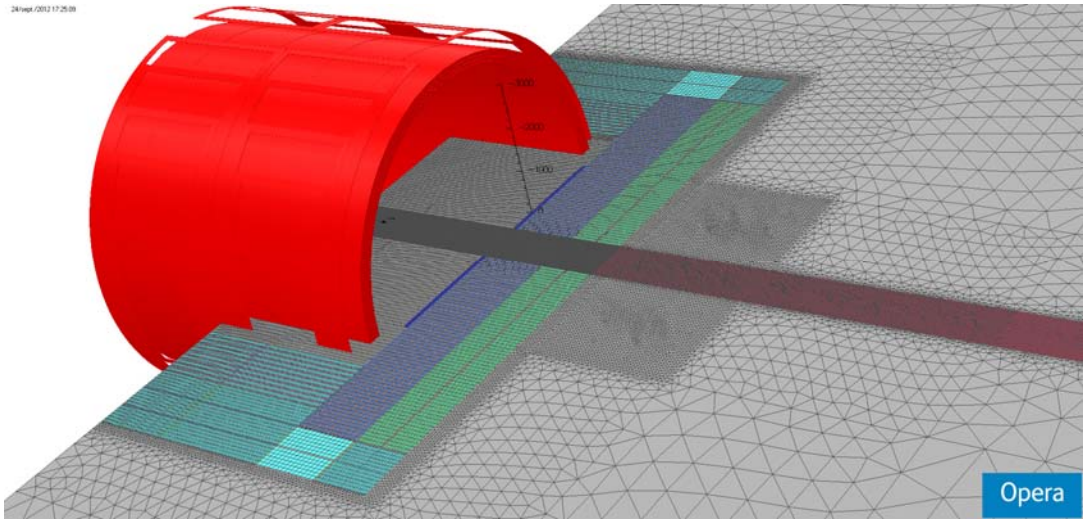

Figure 2: Meshing used in the OPERA-3D simulations.

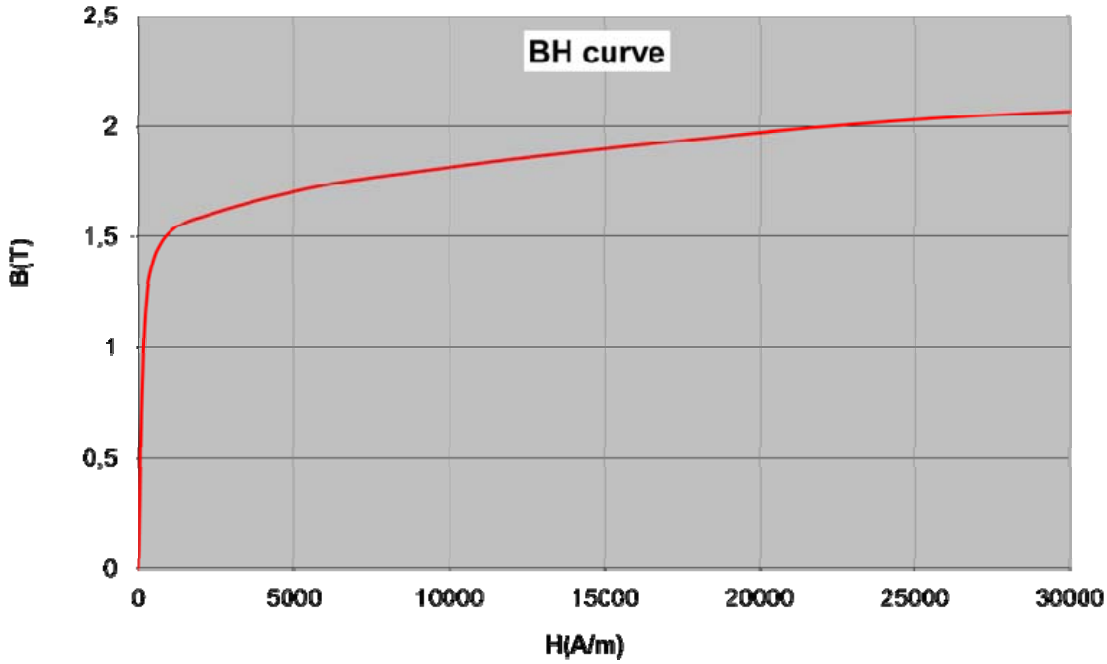

Figure 3: B-H curve for the iron of the yoke, used in the simulations.

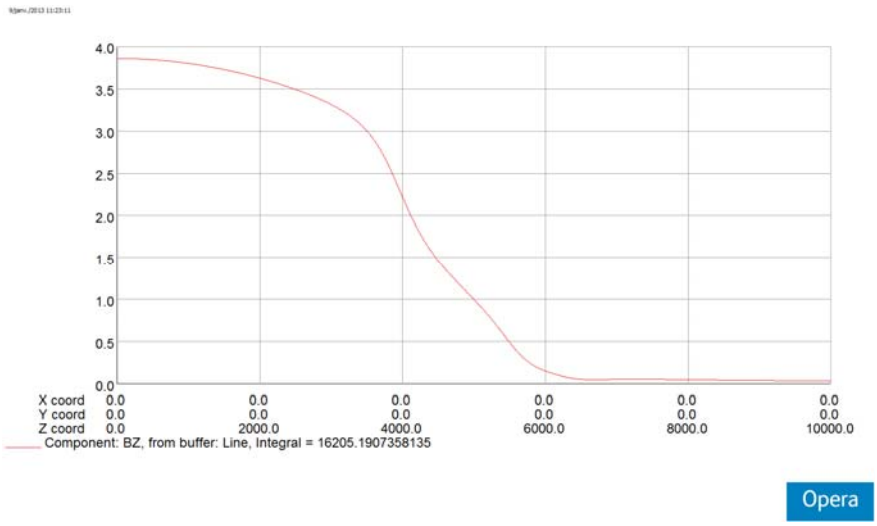

Figure 4: The calculated field B_z along the detector axis. (The field is given in T, the z-coordinate on the horizontal axis is given in mm).

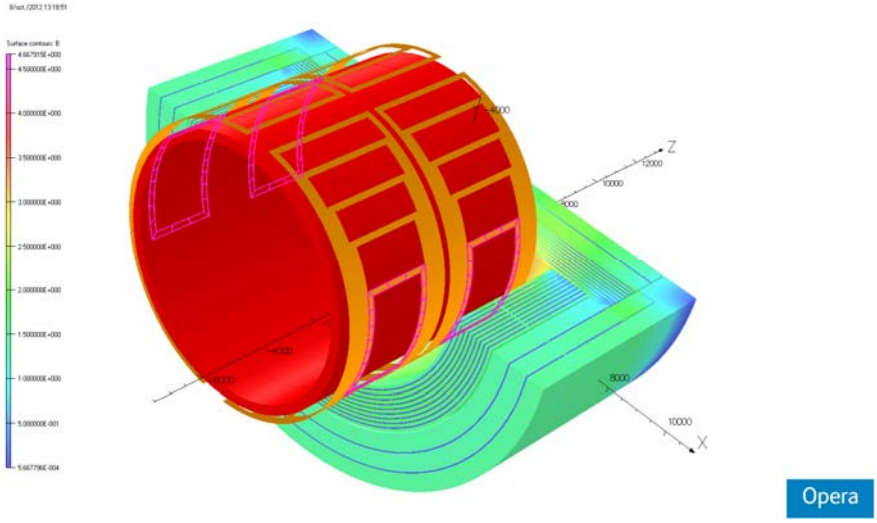

Figure 5: View of the complete ILD magnet system.

4 Solenoid design

4.1 Main parameters and characteristics

The ILD solenoid main parameters are given in Table 2.

The 7.35 m length of the ILD coil enables to make it in 3 modules, each 2.45 m long. The reasons of this choice of 3 modules, rather than 2 or 1, are multiple and concern both easiness of construction and risks: fabrication of the external support, winding and impregnation, transport and handling. Moreover, this enables to have shorter unit lengths of conductor, of about 2.6 km, and to join them in known positions and in low field regions, on the outer radius of the solenoid. Furthermore, with an odd number of modules, the coil mid-plane (Z=0 m), where the axial compressive forces are at a maximum, is not an interface between two modules, therefore limiting the risk of

delamination and heat deposit by friction in the module-to-module coupling region. This is particularly important for the innermost layer, where the field applied to the superconductor is at its maximum.

Each module has 4 layers, with 103 turns per layer. The nominal current is 22.4 kA for the design maximum central field of 4 T.

Tab. 2: ILD solenoid main parameters

Design maximum solenoid central field (T)	4.0	Nominal current (kA)	22.4
Maximum field on conductor (T)	4.6	Total ampere-turns solenoid (MAt)	27.65
Field integral (T*m)	32.65	Inductance (H)	9.2
Coil inner radius (mm)	3615	Stored energy (GJ)	2.3
Coil outer radius (mm)	3970	Stored energy per unit of cold mass (kJ/kg)	13
Coil length (mm)	7350		

The magnetic flux density vector sum of the solenoid is shown in Fig. 6, for a field of 4 T at the interaction point. The model is made using the ANSYS magnetic vector potential formulation with the nodal-based method, and infinite boundaries. The field map of Fig. 6 shows the region of Z=0 to 13m and R=0 to 10m where the coil and the yoke are located. The model is axisymmetric. Taking into account the median transversal plan symmetry, only half of the magnet system is modeled. The coil (and detector) axis is horizontal in Fig. 6.

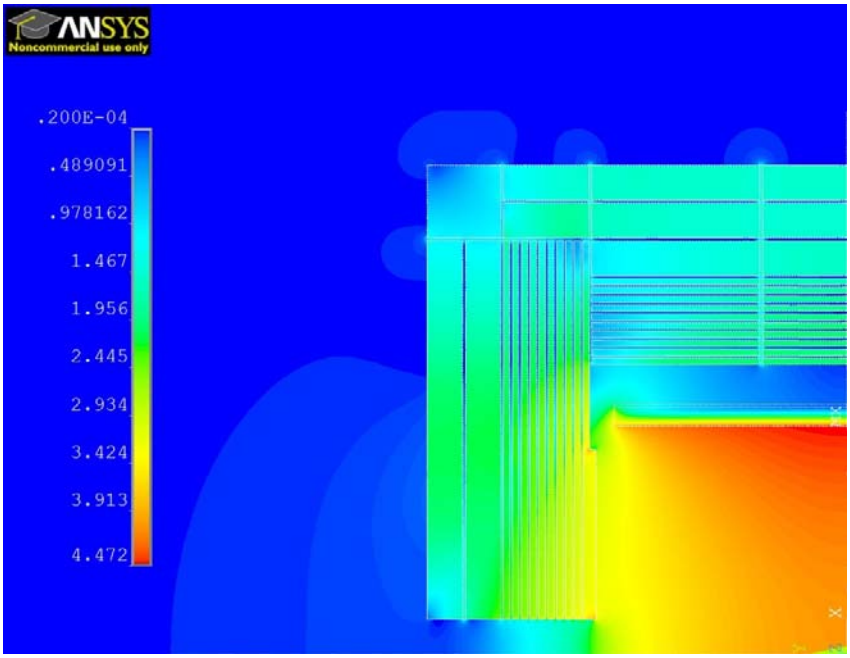

Figure 6: Magnetic field of the magnet system without the anti-DID (numbers given are in T).

4.2 Coil design

4.2.1 Coil structure

A multi-layer coil geometry is required to obtain the 4 T design field with a reasonable nominal current. Similarly to CMS, a 4-layer coil was retained, with a nominal current in the range of 20 kA.

As explained in section 4.1, it was decided to have the coil made in 3 modules of equal length. This choice leaves also the choice to have the modules wound either in external premises or on site.

The coil is wound with the so-called inner winding technique, where an aluminum alloy support cylinder of about 50 mm thickness is used as an external mandrel for the winding. This support cylinder has several important other roles, as it is also used as a mechanical mandrel, a path for the indirect cooling of the coil (with cooling tubes welded on the outer radius of the mandrel, where liquid helium circulates), and a quench back tube (induced currents in this mandrel in case of quench or fast discharge enable a uniform quench of the coil and a limited radial temperature gradient). Both the anti-DID and the tie rods supporting the cold mass will be attached to this support cylinder.

The electromagnetic forces will be contained both by the local reinforcement of the conductor and by the external mandrel. The design has been done to have the same maximum stress and strain in the superconductor reinforcement as in CMS (respectively a Von Mises stress below 145 MPa and a hoop strain below 0.15 %), see section 4.3.

4.2.2 Coil cryostat

The superconducting coil is enclosed in a cryostat, containing also the anti-DID. It consists of a vacuum tank and of thermal shields (inner and outer) covered with multilayer insulation. The vacuum tank, made of stainless steel, is cantilevered from the central ring of the barrel yoke. It is made of two coaxial cylinders joined at their extremities by several wedges.

4.2.3 Coil cooling

The cold mass will be indirectly cooled by saturated liquid helium at 4.5 K, circulating in a thermosiphon mode. This mode, already successfully used for Aleph and CMS, has the advantage of being passive. The description of the thermosiphon mode is given in Fig. 7.

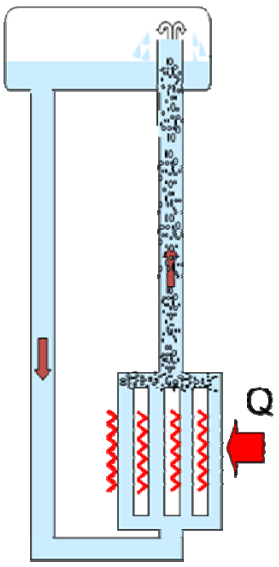

The principle of the thermosiphon is to use the density difference between the pure liquid and a two phase mixture made up of liquid and vapour, as driving head in a U-shaped circuit configuration. A vessel, located in an elevated position, allows the helium-phase separation. The pure liquid is re-cycled to the cooling circuit while the vapour returns to the refrigerator, which continuously supplies the evaporated fraction of liquid

Figure 7: Principle of the CMS thermosiphon.

4.2.4 Support system

Inside the vacuum tank, the coil is supported by 3 sets of tie rods: vertical, radial and longitudinal, similarly to CMS. These tie rods are made of titanium alloy, and dimensioned to support the weight of the cold mass, the forces due to a de-centering of 10 mm maximum of the coil in any direction in the yoke, and the effect of an earthquake up to the local standard safety factor to be applied. The design must also take into consideration the contraction of the coil during cooling and its deformation under magnetic forces.

4.3 Superconducting conductor

The conductor design is similar to the CMS one. It consists of a superconducting Rutherford cable, sheathed in a stabilizer and mechanically reinforced. Two solutions are considered for the reinforcement. The first option is a micro-alloyed material such as the ATLAS central solenoid [5], which acts both as a stabilizer and a mechanical reinforcement. A R&D program on the Al-0.1wt%Ni stabilizer has been launched at CERN and is underway to demonstrate the feasibility of producing a large conductor cross section with this material. The second option is a CMS-type conductor [6] with two aluminum alloy profiles welded by electron beam to the central conductor stabilized with a high purity aluminum. These two options are shown in Fig. 8, together with the actual CMS conductor for comparison.

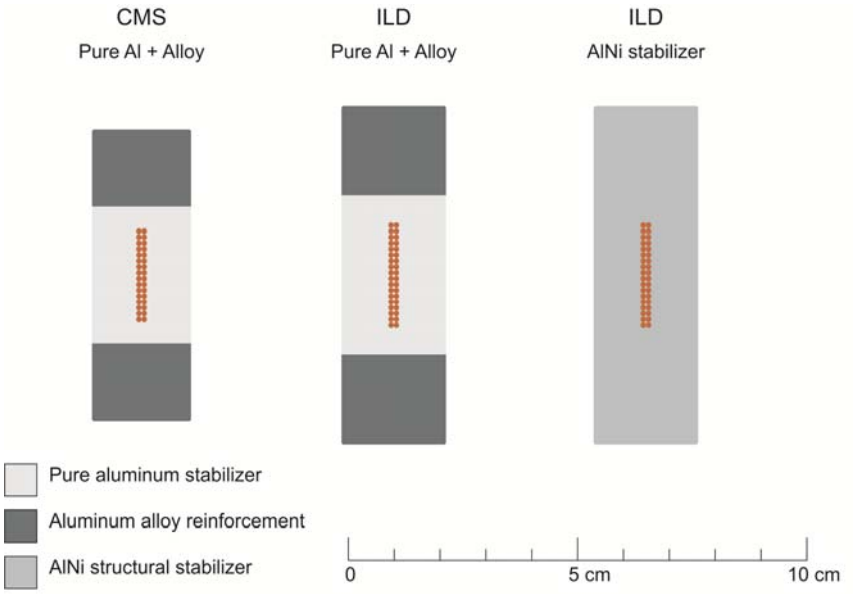

Figure 8: Possible options for the ILD solenoid conductor.

The Rutherford cable will be made with the state-of-the art NbTi superconducting strands. It is proposed to use a cable with characteristics similar to the CMS superconductor, as indicated in table 3 [7, 8].

Table 3. Superconductor characteristics

Superconducting strand in virgin state	
Strand diameter	1.28 mm
(Cu+Barrier)/NbTi	1.1±0.1
SC strand critical current density	3300A/mm^2 at 4.2K, 5T
Rutherford cable	
Number of strand	36
Cable transposition pitch	185 mm
Final conductor	
Overall bare dimensions	74.3 * 22.8 mm^2
SC strand critical current density	≥ 3000A/mm^2 at 4.2K, 5T
Ic Degradation during manufacturing	≈ 7 %
Critical current	67500A at 4.2K, 5T

Compared to the CMS conductor, the number of strands in the cable has been slightly increased to take into account the larger nominal current (36 strands instead of 32), and the conductor width has also been slightly increased to take into account the larger hoop stress. The conductor load line is given in Fig. 9, showing that the temperature margin is around 1.85K, assuming a maximum operation temperature in the coil of 4.5 K. The load line ratio is around 67%.

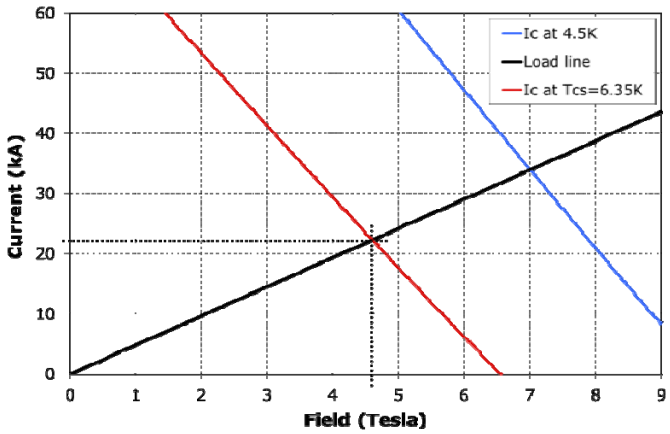

Figure 9: Conductor load line (from CMS strand data).

4.4 Coil protection

In a classical way, the coil protection in case of quench uses an external dump circuit. With a dump voltage of 600 V across the coil terminals, about 56% of the stored energy is discharged outside the magnet in the dump resistor with the pure aluminum stabilized conductor with RRR = 2000 (respectively about 80% with the Al-Ni structural stabilizer with RRR = 590), and the maximum temperature within the coil does not exceed 82 K (resp. 60 K), with an average temperature of 72 K (resp. 56 K). The results are more favorable for the conductor with a structural stabilizer thanks to the larger conducting cross section despite a lower RRR. The comparisons of the current decay and the temperature increase for both conductor options are given in Fig. 10 and Fig. 11 for a fast dump on a resistor of 0.027 ohm.

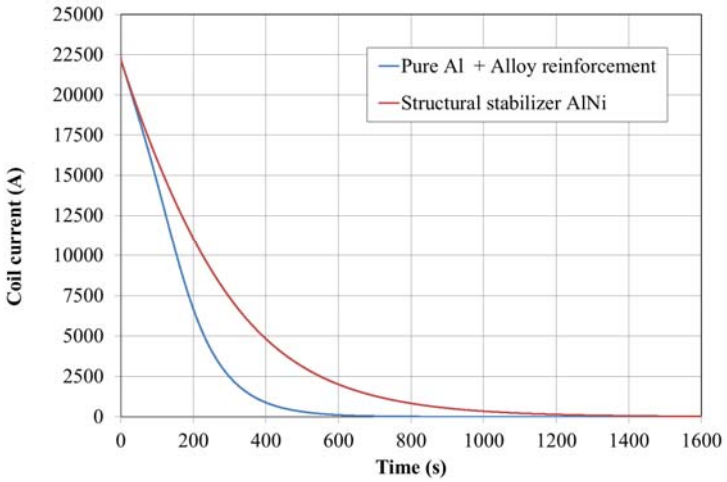

Figure 10: Fast dump of the current on the external resistor for the two conductor options.

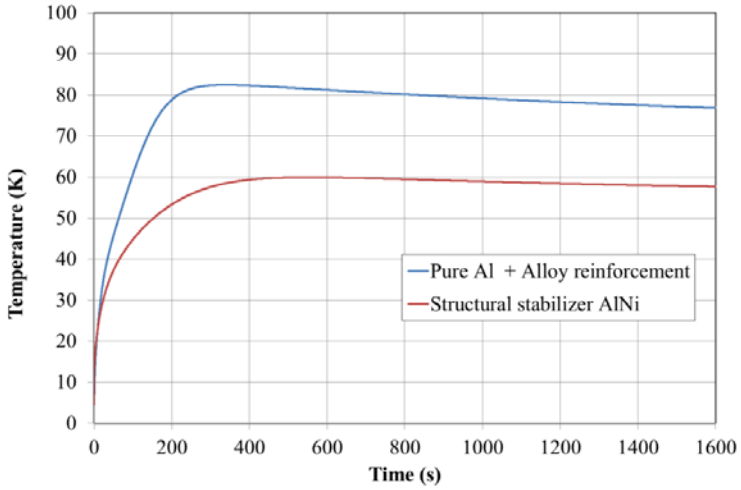

Figure 11: Maximum temperature in the coil during a fast dump for the two conductor options.

Although a large redundancy will be used for both the quench detection and the main switch breakers to fast-dump the magnet energy on the external protection resistor, the fault case of a quench propagating in the coil has been investigated, for the unlikely case that the external dump process is accidentally not activated. The computational results are presented in Fig. 12, where the maximum coil temperature is plotted versus time for a quench initiating at one end of the coil and propagating to the opposite end. The results for both conductor options are given. The temperature reaches 185 K for the pure aluminum stabilized conductor (resp. 150 K for the Al-Ni conductor) and the minimum temperature in the coil in that case is about 65 K, therefore the temperature gradient over the entire coil length stays below 120 K.

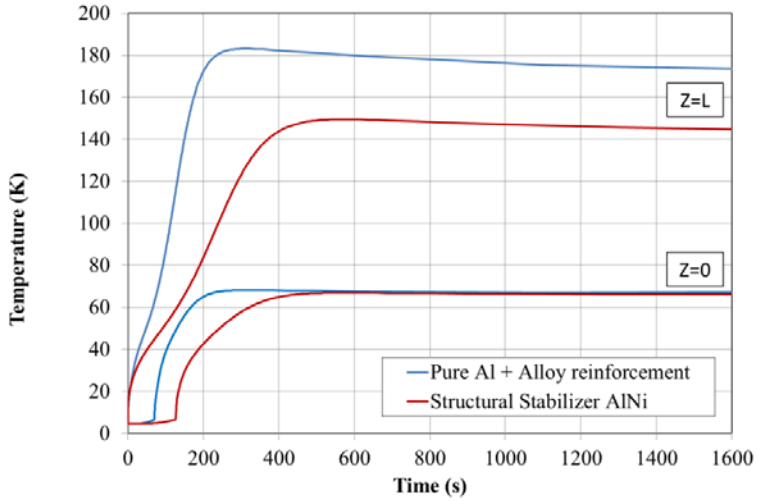

Figure 12: Temperatures in the coil in case of a quench propagating parallel to the coil axis from one coil end at Z=0 to the other at Z=L, for the two conductor options.

5 Anti-DID design

The conceptual design of the anti-DID presented in a very short form in the DBD [1] is described in some more detail in this chapter. For convenience, this version of the anti-DID design is called "Version 1".

Since the completion of the draft DBD in 2012, further studies on the use of the anti-DID in detector benchmark simulations have been done (see Annex A). It is found that version 1 of the anti-DID design does not produce a horizontal field with the distribution exactly as used in the simulations. Therefore, further magnet design studies of the anti-DID were performed. Some preliminary results for a more complex anti-DID design are reported below, called "Version 2".

As an initial result of these studies, it becomes clear that the design of a magnet system including an anti-DID is difficult, in particular if one attempts to provide exactly the field for horizontal steering of background particles as it is used in the detector simulations. Further iterations will be necessary to find the acceptable compromise between the technically feasible and the theoretically desirable.

5.1 Main parameters and characteristics (Version 1)

The requirements on the magnetic field generated by the anti-DID are the following:

- Maximum value of the magnetic dipole field B_x up to 0.035T around z = 3 m from the IP, offering some margin on the final operating field,
- No special requirement from the TPC for the anti-DID field shape around the IP.

The design chosen for the ILD anti-DID is based on a study from B. Parker [9]. The main parameters of the anti-DID are given in Tab. 4.

Tab 4: ILD anti-DID main parameters (version 1)

Design dipole central field on beam axis (T)	0.035	Nominal current (A)	615
Position of max dipole field in z (m)	3	Overall current density (A/mm^2)	40
Maximum field on conductor (T)	2.0	Total ampere-turns anti-DID (kA.t)	656 x 2
Anti DiD inner radius (mm)	4190	Stored energy (MJ)	4.4
Anti DiD total length in Z (mm)	6820	Total inductance (H)	23

5.2 Dipole conceptual design (Version 1)

The anti-DID coil is formed with two dipoles centered on the beam axis with a magnetic field in opposite direction. The angular distribution of the turns is such as to get an approximate cosθ distribution to obtain a homogeneous dipolar field. A 3D view of the anti-DID alone is shown in Fig. 13. The shape of the dipolar field generated for the nominal conditions is shown in Fig. 14.

.

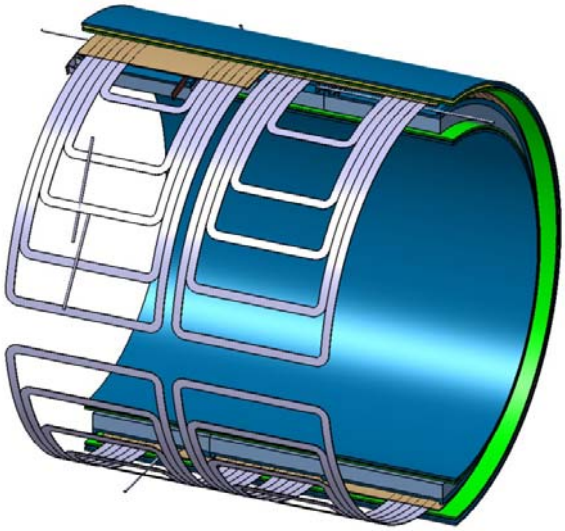

Figure 13: 3D view of the anti-DID (version 1).

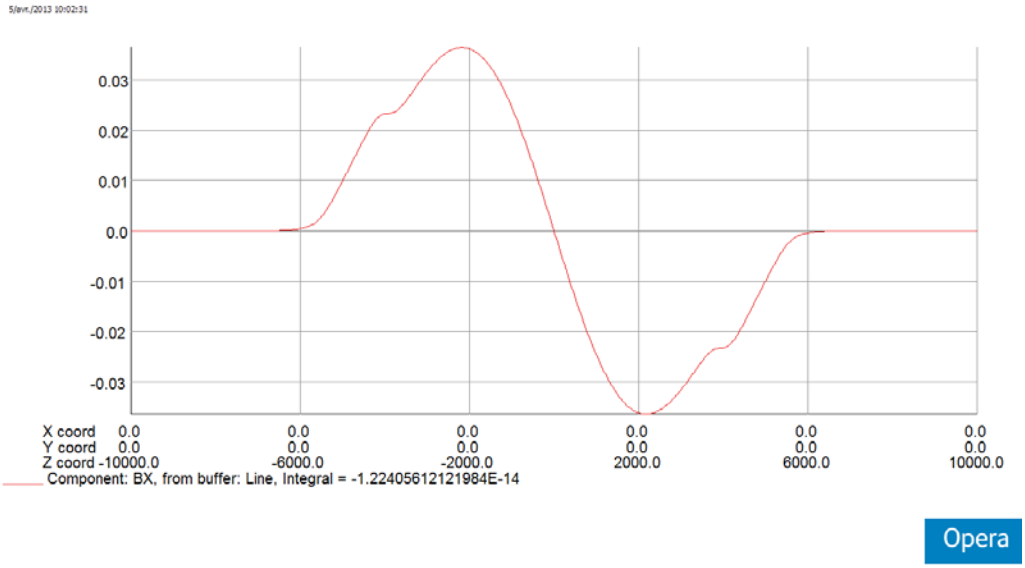

Figure 14: Dipolar field $B_x = f(z)$ generated by the anti-DID (version 1).
(Numbers on the vertical axis for B_x given are in T, labels on the horizontal axis for z are in mm).

For integration reasons, the anti-DID is located within the same cryostat as the main solenoid, and benefits from the cryogenics of the main coil. It is located on the outside radius of the main solenoid, in the lower field region, which is favorable for the temperature margin of the superconductor. The anti-DID coils will be fixed on the mandrel of the solenoid. Details of the design are shown in Fig.15a and Fig. 15b.

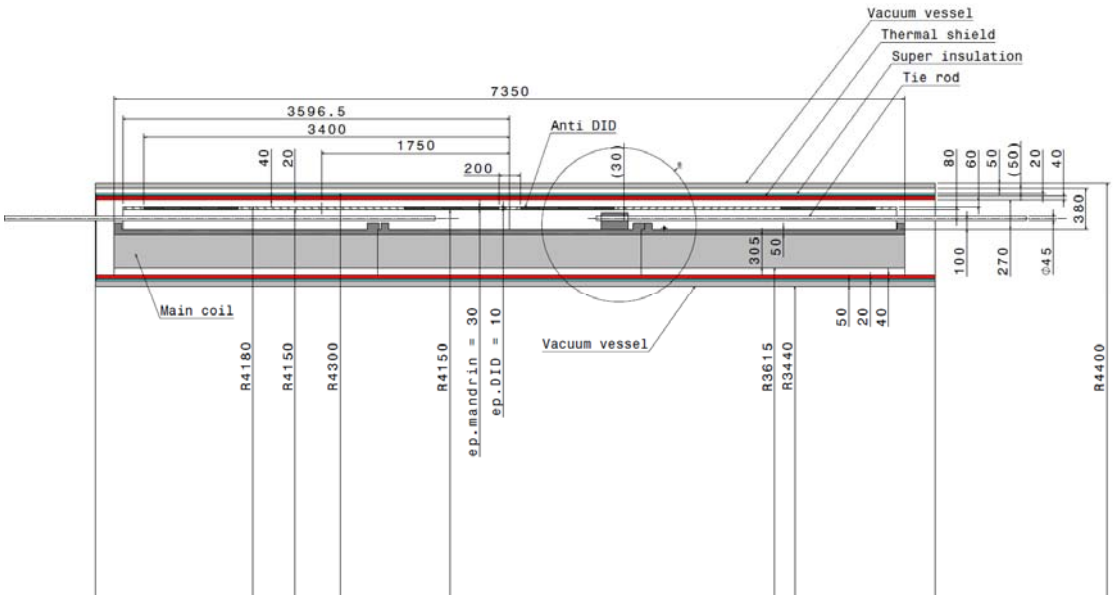

Figure 15a: Integration of the anti-DID in the cold mass.

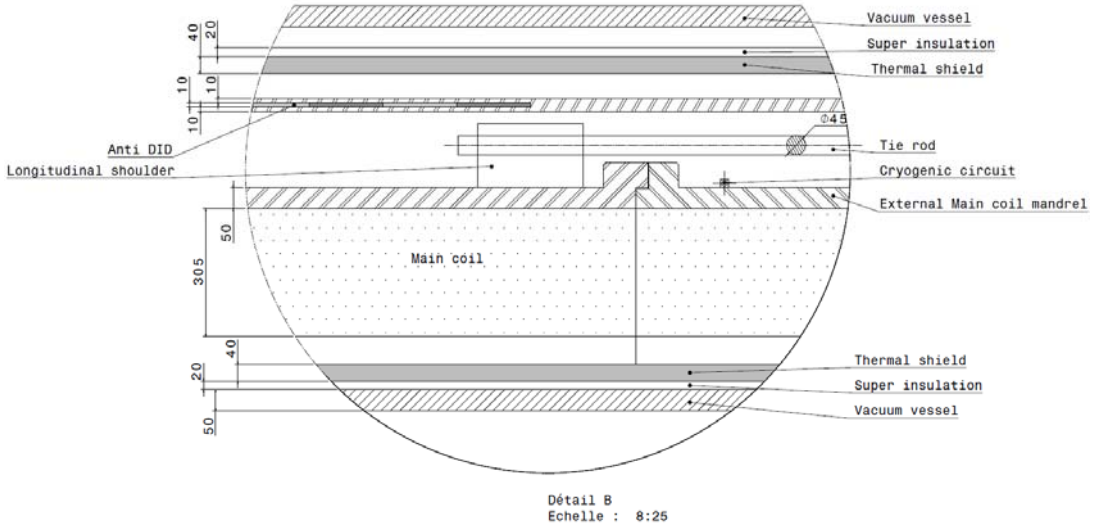

Figure 15b: Integration of the anti-DID in the cold mass (detail B).

The preferred superconductor is NbTi to tolerate some deformation of the winding pack with the cooling from 300 K to 4 K and with the magnetic forces, but other superconductors (like Nb_3Sn and MgB_2) shall be re-evaluated at a more advance stage of the design according to the superconducting technology development. These materials will provide a higher margin in temperature but there is a possible issue with electromagnetic forces and deformation when the main coil is energized, which must be studied. The superconductor shall be aluminum stabilized for protection against quench, as it will be indirectly cooled from cooling tubes, with circulating liquid helium in thermosiphon mode, connected to the same cryogenics supply as the main solenoid. The

conductor could consist of a single CMS strand co-extruded within alloyed-Al. The proposed overall dimension of the conductor is then 4.8 x 3.2 mm^2.

The protection of the anti-DID against quench is achieved by activating heaters to trigger the fast dump of the current. This will bring the whole anti-DID in resistive state to ensure a uniform temperature distribution to avoid a large thermal gradient around the hot spot and limit the associated stresses and distortions. The quench heaters shall also be triggered in case of fast dump of the main solenoid as the refrigeration is stopped in such a case, but inversely, the protection system shall avoid the fast dump of the main coil in case of fast dump of the anti-DID. The possibility to keep the solenoid in operation at 4.5K while the anti-DID is quenched shall be validated.

5.3 Main parameters and characteristics (Version 2)

The requirements on the magnetic field generated by the anti-DID are the following, based on Fig. A4 of Annex A:

- Maximum value of the magnetic dipole field B_x up to 0.035T at z = 3 m from the IP, offering some margin on the final operating field,
- Flat-top of zero magnetic field on about +/- 0.5 m around the IP.

The magnetic design of the anti-DID Version 2 was approached in two steps:

- In the first step, only the anti-DID is taken into account. To get the requested anti-DID field shape, the design is more complicated than for Version 1: each dipole consists of two parts, with different current in each part, and much higher currents than needed for Version 1. The magnetic field obtained for the anti-DID alone (without solenoid and yoke) is shown in Fig 16.

.

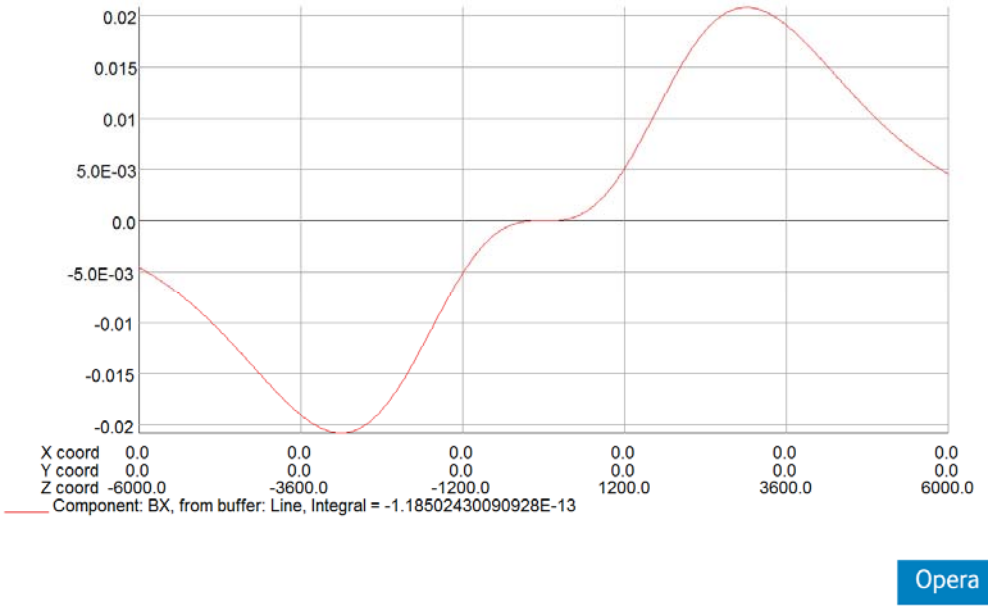

Figure 16: Horizontal magnetic field $B_x = f(z)$ of the anti-DID alone (Version 2). (Numbers on the vertical axis for B_x given are in T, labels on the horizontal axis for z are in mm).

- In the second step, the complete magnetic configuration is taken into account: main solenoid at nominal field, yoke, and anti-DID, with the same currents as for the anti-DID alone. The horizontal magnetic field component obtained in shown in Fig 17.

.

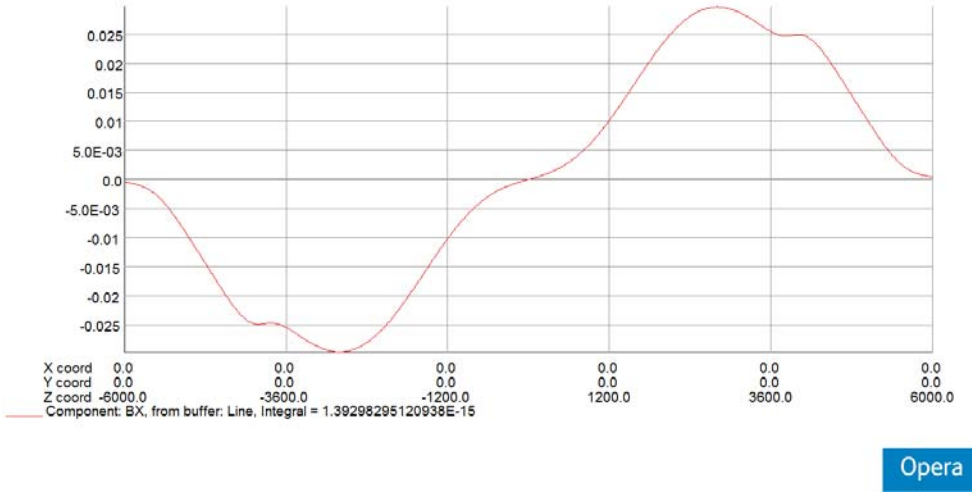

Figure 17: Horizontal magnetic field $B_x = f(z)$ of the anti-DID in the complete magnetic configuration (solenoid, yoke, anti-DID, in Version 2). (Numbers on the vertical axis for B_x given are in T, labels on the horizontal axis for z are in mm).

As was to be expected, a positive effect of the yoke is to increase the magnetic field of the anti-DID by about 50 % (from 0.02 T to about 0.03 T). The position of the maximum B_x remains around 3 m, as required from detector simulations. However, the presence of the yoke deteriorates the field around the IP, and there is no longer any zero-field plateau in this region.

Taking into account the increased complexity (from an engineering point of view) of this Version 2 of the anti-DID, and the fact that it does not reproduce accurately the field B_x as used in the detector simulations, points to the need for further iterations between physics requests and magnet design to find an acceptable compromise design for the anti-DID.

6 Coil manufacturing and assembly

6.1 Solenoid manufacturing

The winding will be done using the inner winding technique, similarly to CMS [10], where the supporting external cylinders are used as external mandrels. These mandrels shall be machined and welded outside of the winding and assembly halls. They shall be built from aluminum plates in aluminum alloy 5083 to get the required 50-mm thickness. Each module flange shall be built from seamless rings using the ring rolling technique [11], to obtain the required uniformity of the mechanical properties in the module connection regions. Several shoulders shall be assembled on the mandrels and used to fix later during the assembly the tie rods and to support the anti-DID. The helium cooling circuit shall be assembled on the mandrel. The cooling circuit shall be designed to withstand both the deformation induced during the cool-down from room temperature to

4.5K and the deformation due to the magnetic forces when the coil is ramped up to the nominal magnetic field.

After the 4 layers of conductor are wound, each module can be vacuum-impregnated. The layer-to-layer electrical joints are made after impregnation. The electrical connections shall be attached on the external mandrels with some degree of freedom to prevent high mechanical stresses on the joints during coil energization.

Then each module can be transferred to the magnet final assembly location.

6.2 Anti-DID manufacturing (Version 1)

The manufacturing of the 4 poles constituting the anti-DID shall be independent from the one of the main solenoid, but it shall be organized and planned in the same timeframe as the main solenoid construction, in order to have the poles and the solenoid available for final test assembly at the manufacturer's premises. The 4 poles will be made of a double-layer winding pack, with a total of 610 turns.

It is proposed to wind the conductor using a coil casing. The coil casing will be built from bent aluminum alloy profiles attached to a dedicated mechanical frame. The casing will allow the winding of the conductor in its final position, using an outer winding technique, and then it will be completed at the end of the winding process to fully clamp the winding pack before the vacuum impregnation. To ensure the mechanical integrity of the coil casing, and the homogeneity of the winding pack, wedges with dummy conductor can be used. Similarly to the ATLAS barrel toroids [12], the use of bladders inflated with pressurized epoxy resin to block the winding pack in the casing shall be investigated. For the completion of the coil casing, bolted or welded solutions can be applied. Welding solutions with low energy deposit and low deformation shall be preferred.

A unique mechanical support frame will be used for coil casing assembly, conductor winding, impregnation, until the anti-DID pole final assembly on the coil, when a complementary structure will be necessary to do the anti-DID pole coupling on the outer mandrel of the main solenoid. These structures will be used for lifting and transportation of the anti-DID poles. A test assembly of the anti-DID pole on a two-module stack of the main solenoid shall be done at the manufacturer's premises. The strain relief of the coil casing during coil curing shall be looked at.

The winding procedure and tooling shall be validated with a winding test of a prototype using a dummy conductor. The dimensional tolerances that can be obtained with the manufacturing process shall be checked on the prototype.

6.3 Coils assembly

The proposed assembly of the coil is similar to the CMS's one [13]. The three modules of the main solenoid will be assembled in a surface hall on the ILC site near the access to the experimental area. They will be stacked vertically for the mechanical coupling. Special care is needed to ensure the flatness of the contact surface between two adjacent modules. The electrical joints and helium tubing will be connected before the assembly of the anti-DID. After the completion of the solenoid assembly, the final assembly of the anti-DID poles can take place. They will be fixed on the main solenoid in the same vertical position. The mechanical coupling of the poles will be made on dedicated shoulders located on the external radius of the main solenoid mandrel. The

mechanical support frame of each anti-DID pole will be removed after their fixing on the mandrel. This mechanical coupling will be designed to allow both the deformations due to the thermal shrinking during cool down from room temperature to 4K, and the deformation of the main solenoid when it is energized. The electrical joints of the conductors of the 4 poles shall be done in a similar way as the joints between the layers and modules of the main solenoid. The helium tubing of the anti-DID will be connected to the main refrigerator helium feeding manifolds.

After the installation of the thermal screens and the multilayer insulation on the coils in vertical position, the cold mass is swiveled to the horizontal position on its supporting platform, and inserted into the outer cylinder of the vacuum tank which is fixed in cantilever to the central yoke barrel. The coil is then attached to the outer cylinder of the cryostat with several longitudinal and radial tie rods.

7 Ancillaries

7.1 Power circuit

The power circuit must include a dump resistor always connected to the coil to ensure the safe discharge of the magnetic energy when opening the main switch breaker which connects the power supply to the coil.

The power supplies will allow to ramp up the current with a controlled rate for a typical total ramp up duration of about 4 hours. A two-quadrant converter will offer the possibility to ramp down the field to intermediate values for intervention. The nominal current will be delivered with a precision of a few ppm. The converters will be located in the underground service area, to limit the voltage drop on the powering lines.

A high temperature superconducting (HTS) link is the preferred option for the flexible power lines. Such a line is cooled by the helium gas coming from the coil back to the refrigerator, with a temperature between 5 K and 20 K. These flexible lines can be permanently connected to the magnet both for the on-beam and garage positions. The bending radius of the HTS power lines has to be known to finalize the integration studies to allow the movement from the garage to the on-beam position. Compared to the conventional copper busbars, the HTS line has less power dissipation and is less heavy and massive, an advantage as far as support and integration are concerned.

It is envisaged to do the connection between the superconducting coils (main solenoid and anti-DiD) and the HTS power lines with superconducting busbars with a Nb3Sn cable stabilized with copper, and with helium cooling at 4.5 K, located inside a specific chimney across the yoke thickness. The diameter of this chimney will therefore be smaller in comparison to the conventional copper current leads having one extremity at room temperature.

The current leads shall be built as well with HTS superconductor. They will be located outside the yoke. Two pairs of current leads are needed: one pair to connect the dump resistor on top of the yoke, the other pair in the service area at the other extremity of the HTS power lines to connect to the power converter.

The dump resistor must be designed to dissipate either the full magnetic energy in case of slow dump (SD) with a time constant of about 9300 s, a peak power around 500 kW and a resistor of 1 milli-ohm for the solenoid, or about half of the magnetic energy in case of fast dump (FD) with a time constant about 177 s with the pure aluminum stabilized conductor option (resp. 274 s with the AlNi stabilizer option), a peak power around 13MW and a resistor of 27 milli-ohm for the solenoid. The power lines connecting the current leads to the dump resistor must be sturdy enough against the SD and FD even in case of failure of their cooling system. The dump resistor shall preferably be located near the top of the magnet to ensure the magnet discharge even in case of fault on the HTS flexible power lines. The resistor design shall be compact, with two configurations for the SD and the FD, selected with locally installed power contactors. A conceptual design of a dump resistor is described in [14].

The main switch breakers shall be doubled for safety. They will be located in the service underground area near the power supply.

The anti-DID will have its own power circuit with similar characteristics as the one described for the main coil (power supply, HTS power lines, current leads, dump resistor). The same chimney will be used for both the solenoid and the anti-DID power lines. The sketch of the powering circuits is given in Fig. 18.

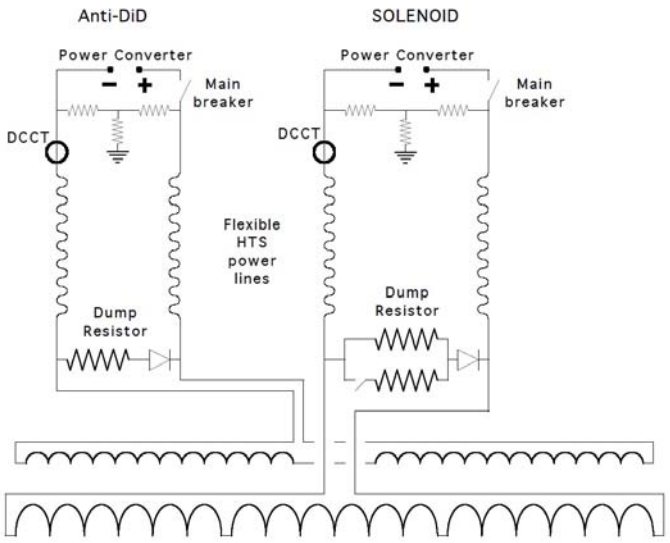

Figure 18: Powering circuits of the solenoid and the anti-DiD.

7.2 Control and safety systems

These systems are of a standard type and consist of two parts, which are independent, but exchange information between each other [15].

7.2.1 Magnet Safety System (MSS)

The MSS continuously measures safety parameters and magnet status in order to prevent operation in dangerous conditions. In particular, it shall trigger a fast discharge of the magnet for conditions potentially generating a quench of the coil. The safety signals are analog ones, coming from quench detectors (QD) and voltage taps. They are

transferred for treatment to an analog chassis, using hardwired connections. No feedback path, no bus system and no software programs are used for this part.

For safety reasons, the QD comparing the voltage across the coil parts must be redundant, typically 2x3 QDs for the solenoid and 2x4 QDs for the anti-DID. Additional QDs and voltage taps are used to protect the busbars and the current leads.

7.2.2 Magnet Control System (MCS)

The MCS provides the controls needed to execute the automatic processes of the various running modes of the magnet system for all operation phases. It is based on PLC and control software.

More diagnostic systems, useful for a better comprehension of the magnet behaviour can be added. Typical examples are:

- Constructor Diagnostic System (CDS), useful for measuring non essential parameters during the first test of the magnet, including the cool-down, and useful in case of problems,
- Magnet Diagnostic System (MDS), with a high speed data acquisition, continuously refreshed, and storage only in case of quench for a further post-quench analysis.

7.3 Cryogenic plant

The implementation of the cryogenic plant will strongly depend on the site choice. Some general principles are nevertheless proposed in this chapter.

A solution where ILD has its own cold box, rather than a single cold box supplying both experiments ILD and SiD, is preferred [16]. The same refrigerator will be used to cool down ILD solenoid and the anti-DID. It shall also be able to extract the dynamic losses during the various magnet ramps or discharges. The different parts of the plant are:

- Compressors, with gas He tank storage, and LN2 tank for pre-cooling and compressed air back up for the pneumatic valves;
- Helium liquefier in the underground area, supplying the liquid helium to the coils and taking the helium gas return back from the coils and the power lines, possibly in a position close to the magnet compatible with the fringing field and the maintenance activities.

The proximity cryogenics is on top of the magnet for the thermosiphon refrigerating mode, with:

- The dewar containing a spare volume of LHe to keep the magnet at nominal field in case of temporary disruption of LHe supply, and to allow the ramp down to zero field keeping the magnet in superconducting state;
- The valve box;
- The phase separator to feed the thermosiphon of both the solenoid and the anti-DiD.

Depending on the position of the cold box, a flexible vacuum line may be used to connect the liquefier to the proximity cryogenics.

The heat load is estimated to be around 400 W @ 4.5 K [16], but the refrigerator shall be dimensioned taking into account the acceptable cool-down time. Moreover, losses during ramping the magnet up and down, and the losses in the current leads must be taken into account for dimensioning the refrigeration plant, with some safety margin.

8 Magnet tests and field mapping

8.1 Magnet tests

A full test of the magnet at its nominal current is mandatory before the inner detectors are installed. This test requires that the yoke is fully mounted around the cold mass. This test will first enable to check all functionalities of the coils and their ancillaries at the nominal field and in the stray field. It is also necessary to make a complete field mapping of the magnet, up to its design field.

The typical points to be controlled are:

- To check the slow and fast discharges at increasing currents;
- To check the behaviour of the ancillaries for each transient (charges-discharges);
- To control the cryogenic safety (pressure rise) and the electrical safety (voltage drops, ground insulation);
- To evaluate the stability margin, by increasing the inlet He temperature;
- To set the He flow in the current leads as a function of magnet current, including helium flow at zero current;
- To monitor all magnet parameters (stress, temperature, voltage, resistances of joints, etc.);
- To measure the magnet inductance as a function of current (this value decreases with the iron saturation).

8.2 Field mapping

The field mapping is a very important step of the magnet tests. The coil inner bore volume will have to be mapped. The B-field map will have to be measured to about 1 G in an overall field of 4 T [17], i.e. with a relative accuracy around 2.E-5, which is very challenging. For CMS, the Hall probe calibration was done with an accuracy of 5.E-4, and the accuracy on the B_z measurement was estimated to 7.E-4 [16]. An NMR probe will provide the absolute reference.

Possibilities to increase the measurement accuracy could be to increase the number of measurement points during the field mapping (the measurement accuracy increases roughly as $\sqrt{N}$, N being the total number of measurements), or to use a differential method.

The differential method is commonly used to measure harmonics in an accelerator magnet. For the application to a solenoid, one can imagine two Hall probes put in opposition:

- the external one measures the 3 field components, B_z, B_x, B_y;
- the central one measures only the B_z component;
- by putting the two signals in opposition, only the minor components B_x and B_y are remaining in the signal.

This option should be studied in more detail, also taking into account the field generated by the anti-DID.

9 Iron Yoke Design

The yoke has several functions. It provides the flux return of the solenoidal field and reduces the outside stray fields to an acceptable level. It is instrumented with detectors for muon identification and tail catching of hadronic showers. In addition, the yoke is the main mechanical structure of the detector. The ability for access and work in the interaction region (IR) hall during beam operation requires the detector to be self-shielding. The design allows for a fast opening in order to get access to the inner detector components.

For the inner part of the yoke a fine segmentation of the iron was chosen, 10 layers of 100 mm thick plates with 40mm gaps for detectors to be inserted for good muon reconstruction, rejection of hadron background and good performance of the tail catcher. This segmentation is in particular useful for the tail catcher, whereas a similar performance of the muon system could be achieved by arranging the detectors in groups of layers. In addition to the inner fine segmentation, some 560 mm steel plates are added on the outer part mainly to reduce the stray field.

During beam operation the IR hall has to be accessible due to the push-pull concept. Since all activities in a high magnetic field are very cumbersome and potentially dangerous, a field limit of 50 G at 15 m radial distance from the beam line was agreed upon [18]. Two- and three-dimensional FEM field calculations were done using the CST EM Studio program, varying the thickness and geometry of the iron in the barrel and end-caps until the goal of less than 50 G at 15 m radial distance was achieved. This was obtained with three 560 mm thick steel plates in the barrel and two 560 mm plates in each end-cap in addition to the ten 100 mm thick inner layers. This results in a total thickness of the iron of 2.68 m in the barrel and 2.12 m in the end-caps, respectively. In order to obtain the desired limit, all gaps between the steel plates on the outer radius have to be closed with iron. The only exceptions are the gaps between the barrel rings and between barrel and end-caps. This space will be needed for cables, cooling pipes and other services.

It should be noted, that the field calculations assume no additional magnetic material outside the yoke and that the results are at the limit of the accuracy of the FEM calculations.

The strong magnetic field, maximum of 4 T, introduces large magnetic forces on the end-caps, which were calculated using different FEM programs (CST EM Studio and ANSYS). The largest force, an inward pulling force in the z-direction of about 180 MN, acts on each end-cap, which has to be taken into account in the mechanical design.

9.1 Barrel yoke design

The solenoid with the central subdetectors is supported by the central barrel ring, the only stationary part around the interaction point. Both outer rings can be moved independently along the z-direction to allow access to muon chambers and services. A dodecagonal shape was chosen in order to reduce the weight and size of the sections. The twelve segments come in two slightly different sizes to avoid segment edges pointing towards the beam line. The average weight of a segment is about 190 t. Figure 19 gives an overview of the design.

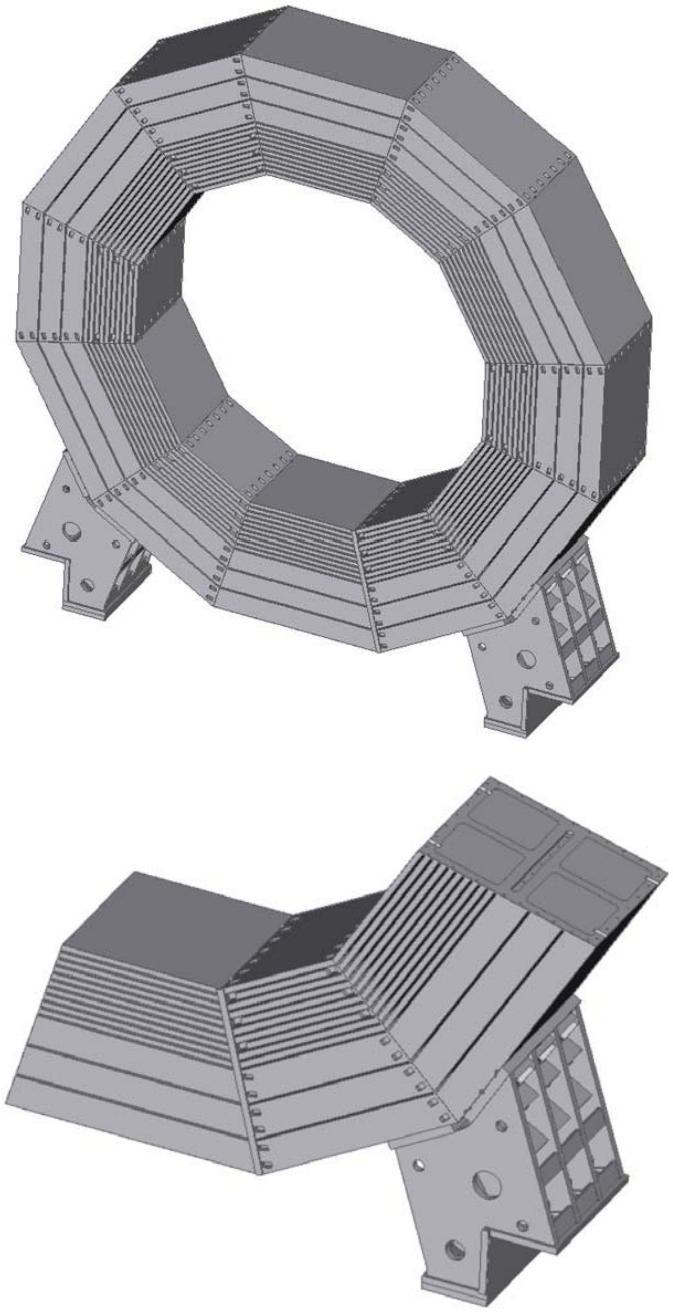

Figure 19: The yoke barrel design: general view of one barrel ring (top) and detailed view of a sector with one supporting foot (bottom).

The 10 plates of an inner segment and the three outer plates are welded together with 30 x 40 mm spacers between the plates along the segment edges. Segments are then bolted together on all sides using M36 bolts (bigger on outside). Shear keys between the segments prevent radial displacement, whereas shear pins on the inner and outer edges are used to prevent movements along the z-direction.

The fully assembled barrel ring is a very stiff structure. The maximum vertical deformation of an outer ring is 1.6 mm, which is due to the gravitational load. At the very end of the coil there is a radial magnetic field component acting on the inner plate of the outer ring, which introduces a force of about 1.3 MN. This leads to a 1.5 mm radial deformation of the plate.

Each barrel ring has a mass of about 2300 t, including the support feed. The central barrel ring has to carry an additional weight of almost 1000 t, the mass the cryostat with the coil, barrel calorimeters and central tracking detectors. For the calculation of deformation and stress the cryostat was approximated by a single 50 mm thick steel cylinder attached to the barrel at 12 points. The additional gravitational load was introduced by increasing the density of the cylinder. The maximum vertical deformation is 4 mm.

9.2 End-cap yoke design

The design of the end-cap is more challenging compared to the barrel due to the large magnetic forces, about 180 MN acting in the z-direction. Several geometries were considered. A design with radial supports instead of horizontal supports was chosen due to the larger second moment of area, better transfer of force to the barrel, symmetric iron distribution and a minimum of dead material. This design minimises the end-cap deformation and stress. An overview of the design is shown in Figure 18. The end-cap is made out of twelve wedge-shaped segments, extending from the inner hole to the outside of the yoke, consisting of 10 inner 100 mm thick plates, and two outer plates 560 mm thick. In addition, a 100 mm thick steel plate was introduced to improve the self-shielding of the detector.

Similar to the barrel, the 10 plates of an inner segment are welded together with spacers along the segment edges, thus forming rigid structures, with the spacers acting as supports. Segments are then bolted together on the front and back sides using M36 bolts. A central cylindrical support tube of 1.0 m (1.2 m) inner (outer) diameter is bolted to the individual inner and outer plates, making a rigid connection of the inner and outer parts.

The maximum deformation of the end-cap due to the magnetic force of 180 MN is about 3 mm. The forces are transmitted to the barrel through z-stops the resulting stress is less than 200 MPa. The total weight of one end-cap is about 3250 t.

9.2 Yoke assembly

After a full trial assembly at the manufacturer, the barrel and end-cap segments with a maximum weight of 200 and 90 t, respectively, are transported to the experimental site. In case of vertical access shaft, the assembly the barrel rings and end-caps is done in the surface building above the IR region. Complete barrel rings and the end-caps are then lowered into the IR hall, similar to the CMS assembly.

The design does not have to be changed for a mountain site with horizontal access tunnels. Barrel and end-cap segments have to be transported into the IR hall, where the rings and end-caps are then assembled. This requires more work and time spent in the IR hall and requires a 250 t crane in the IR hall.

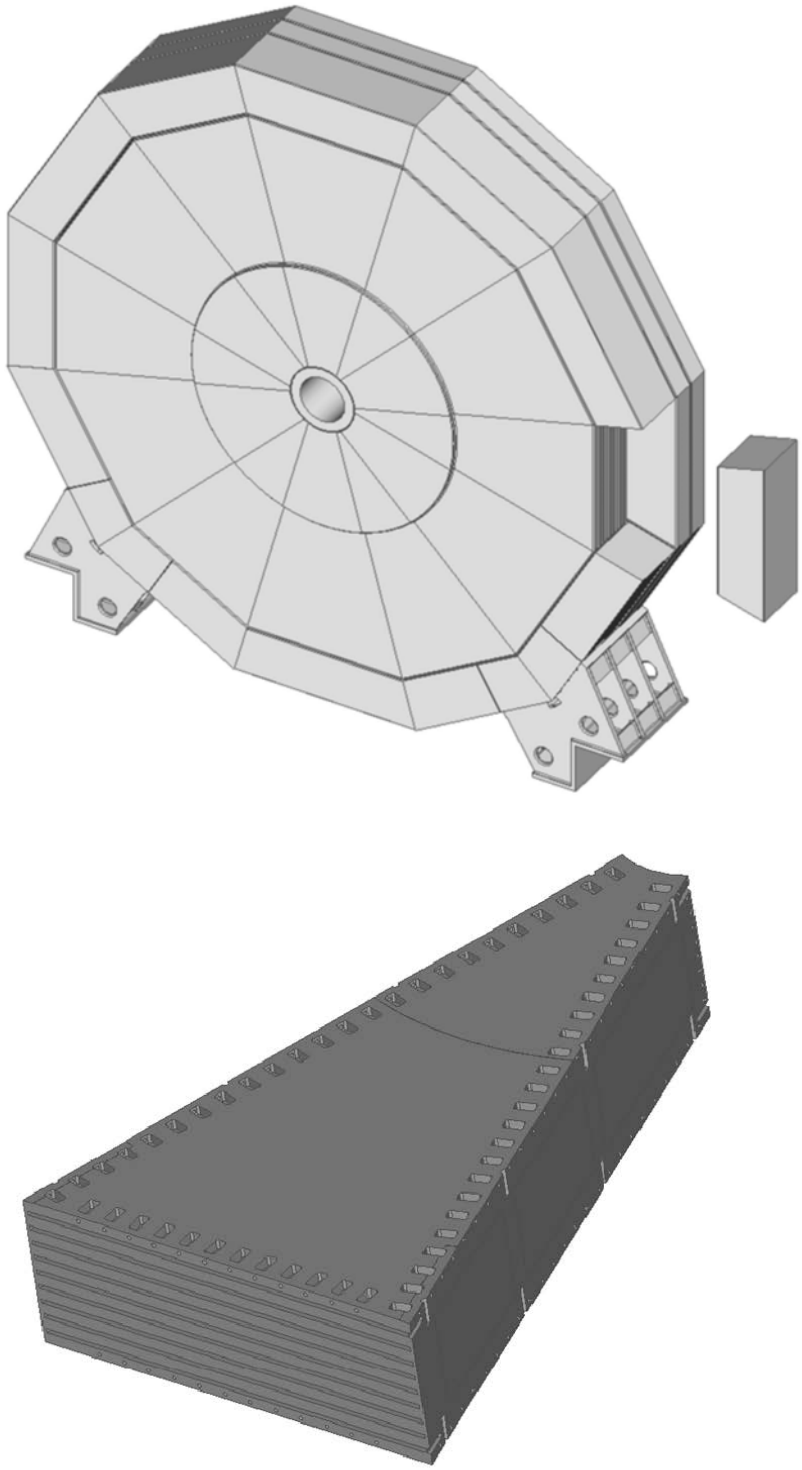

Figure 20: The yoke end-cap design: overview (top) and detailed view of the design of one sector (bottom).

10 Summary

The study reported here shows that the 4 T ILD superconducting solenoid with a 7.35 m length and 6.88 m diameter warm aperture, and including a superconducting anti-DID, is feasible. Except for its dimensions and the presence of the anti-DID, this magnet is similar to the CMS one, so it is not surprising that many technical solutions already used for CMS are proposed here. The main improvement would be to modify the structure of the reinforced superconductor, using a micro-alloyed material for the reinforcement. Some other improvements proposed are the use of HTS materials for the current leads, the bus-bars, and eventually, the anti-DID.

A preliminary design of an anti-DID included in the cold mass is proposed. More discussion within the ILD community, and a few iterations between detector simulations and magnet design work, are needed to advance towards a final anti-DID design.

In addition, a design of the iron yoke is presented, which fulfills all the requirements.

11 Acknowledgments

The authors are grateful to the ILD collaboration for its continuous support during the period of this study, and to many of its members for specific discussions.

12 References

[1] ILD Concept Group, International Large Detector DBD, December 2012
[2] T. Behnke et al., *ILC Reference Design Report Volume 4 – Detectors*, (2007) arXiv:0712.2356
[3] R. Settles, LCTPC and the Magnetic Field for ILD, LC-DET-2011-002
[4] F. Kircher et al., CMS Coil Design and Assembly, IEEE Trans. Appl. Superconductivity, Vol. 12, No 1, Mar. 2002, 395-398
[5] K. Wada et al., Development of High-Strength and High-RRR Aluminium-Stabilized Superconductor for the ATLAS thin Solenoid, IEEE Trans. Appl. Superconductivity, Vol. 10,No 1, Mar. 2000, 373-376
[6] B. Blau et al., The CMS Conductor, IEEE Trans. Appl. Superconductivity, Vol. 12,No 1, Mar. 2002, 345-348
[7] B. Curé et al., The superconducting strand for the CMS solenoid conductor, IEEE Trans. Appl. Supercond., vol. 12, No. 1, pp. 1014–1017, March 2002.
[8] P. Fabbricatore et al., Electrical characterization of S/C conductor for the CMS solenoid, IEEE Trans. Appl. Supercond., vol. 15, No. 2, pp. 1275–1278, June 2005.
[9] B. Parker, private communication, September 2008
[10] P. Fabbricatore et al., The Manufacture of Modules for CMS Coil, IEEE Trans. Appl. Superconductivity, Vol. 16,No 2, June. 2006, 512-516
[11] S. Sgobba et al., Design, construction and quality tests of the large Al alloy mandrels for the CMS Reinforced Conductor, IEEE Trans. Appl. Superconduct., Vol 12, 428-431, Mar. 2002.
[12] J.M. Rey et al., Cold Mass Integration of the ATLAS Barrel Toroid Magnets at CERN, IEEE Trans. Appl. Superconductivity, Vol. 16, No 2, June 2006, 553-556
[13] B. Levesy et al., CMS Solenoid Assembly, IEEE Trans. Appl. Superconductivity, Vol. 16, No 2, June 2006, 517-520

[14] A. Gaddi and F. Duarte Ramos, Design of a Compact Dump Resistor System for an LCD Magnet, https://edms.cern.ch/document/1074886/
[15] G. Maire et al., LHC Experiments Magnets Control Project, unpublished, September 2005
[16] T. Okamura et al. Cryogenic System of Interaction Region in the Japanese Mountain Site, Webex meeting, June 1st, 2012
[17] V. Klyukhin et al., Measurement of the CMS Magnetic Field, IEEE Trans. Appl. Superconductivity, Vol. 18, No 2, June 2008, 395-598
[18] B. Parker, A. Mikhailichenko, K. Buesser, J. Hauptman, T. Tauchi, et al., Functional Requirements on the Design of the Detectors and the Interaction Region of an e+ e- Linear Collider with a Push-Pull Arrangement of Detectors, SLAC-PUB-13657, ILC-NOTE-2009-050

Annex A: Remarks concerning the anti-DID

This annex attempts to summarize the developments at ILC, and in the ILC detector concepts, concerning the anti-DID (detector-integrated dipole). The main purpose here is to explain the choice of specifications for the anti-DID field strength and field shape adopted for the DBD of ILD (cf. chapter 5 of this note).

Early discussions about a detector-integrated dipole (DID) were initiated when the adverse effects of a crossing angle of the beam at the IP of a linear e^+e^- collider became evident [A1]. A DID would have been able to compensate, to some extent, for the steering of the beams passing at an angle in the strong solenoid field of the experiment at the interaction point. In addition, a DID would help reduce spin precession of the polarised beams in the detector region.

Later, it became clear that such DID fields would have a considerable negative impact on the number of background hits (in particular from back-scattering particles) in the inner detectors of the experiment. Instead, it was found that a DID with inverted polarity, a so-called "anti-DID", would allow to steer background particles towards the exit holes (outgoing beam pipes) of the experiment, thus reducing the back-scattering. At the same time, remaining backscattering particles are guided to spiral back through the center of the detector, thus avoiding e.g. to hit the vertex detector layers.

The ILC RDR (2007), Volume 4 on Detectors [A2], mentions the anti-DID in several places, as the "preferred solution" (over the DID). No details concerning field strength or shape nor any reference is given.

The ILD LoI (2009) [A3] mentions the anti-DID in the TPC section, with a reference to the accurate magnetic field measurements needed before installation of the inner detectors. No details or reference concerning the shape and strength of the anti-DID magnetic field are given.[1]

A more detailed paper was published by A. Seryi et al. in January 2006 [A5]. It describes the DID and anti-DID fields in the context of an overall IR optimization. The three detector concepts discussed at the time, SiD, GLD and LDC, are considered in the study. As shown in Figure A1, below, for SiD the anti-DID peaks at around 1.8 m, with a value of 0.02 T. The anti-DID fields assumed for GLD and LDC peak around z = 3 m, with maximum values of about 0.02 T and 0.035 T, respectively.[2] Detailed tables of the magnetic fields for the three detector concepts, resulting from the study [A5], are given

[1] The SiD LoI [A4] provides, on page 66, a conceptual design and a plot showing the B_x field along the detector axis. In this preliminary design, the anti-DID field in SiD peaks at about 1.8 m with a value of 0.06 T.

[2] Later, D. Toprek and Y. Nosochkov [A8] investigated the effect on the disrupted beam of the anti-DID in SiD, i.e. the beam after the IP, with particular attention given to the compensation of the anti-DID for the measurements at the down-stream polarimeter. A set of dipole correctors on top of the extraction line quadrupoles was found to be necessary. In this study, the anti-DID field in SiD peaks at approx. 1.8 m with a value of 0.02 T.

in [A6]. A presentation by A. Seryi, which contains a description of luminosity loss due to the anti-DID, can also be found in [A6]. Here, it was pointed out that one might want to operate the anti-DID in LDC **at 30% below** the value for optimal background reduction, in order to reduce the expected luminosity loss from about 5% to about 2%. It must be noted that, at a later stage (for the LoI), the anti-DID field for SiD was revised (see Figure A2.)

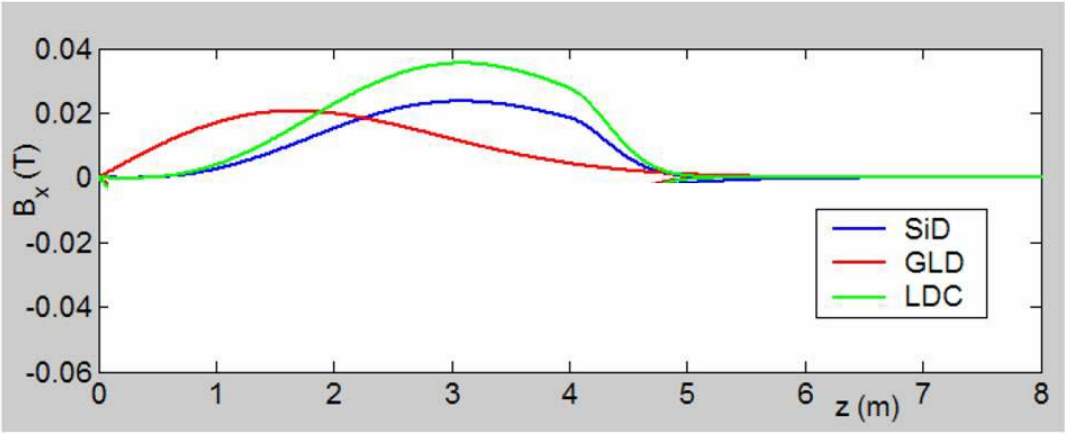

Figure A1: Anti-DID field strengths suggested in 2006 (copied from [A5]).

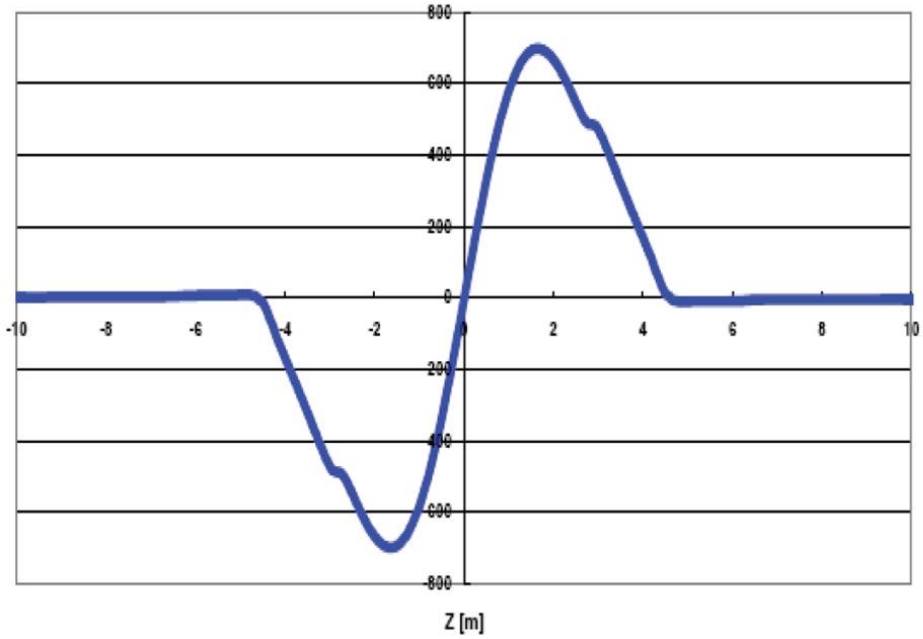

Figure A2: Anti-DID field for SiD, as shown in the LoI of 2009 (copied from [A4]). The field peaks at around 700 Gauss (vertical axis not labelled in [A4]).

It should be noted that the 2006 paper [A5] puts weight on improving the anti-DID field shape for detector concepts using a TPC. This was later found to be of little importance - a very precisely measured field map is now deemed to be sufficient for operating a detector with a TPC, independently of the presence on an anti-DID [A7].

Detailed information on the anti-DID for LDC, and its effect on background in the detector, can be found in A. Vogel's thesis [A9], and references therein. In this work, the anti-DID field as proposed by A. Seryi [A6] has been used (see Figure A3), **without** the optional 30% reduction of field strength (to reduce luminosity loss). In terms of software implementation, the MOKKA magnetic field description ***fieldX01***was used throughout this thesis. (For later versions of MOKKA fields, see below). Also according to this thesis (in its appendix C3.3.3), there is a possibility to moderately scale the anti-DID field by changing ***fieldvalue*** inside the ***fieldType 6*** (kMapDID). For his thesis, A. Vogel used a ***fieldvalue*** of 1.0 (see table D.3 in [A9]).

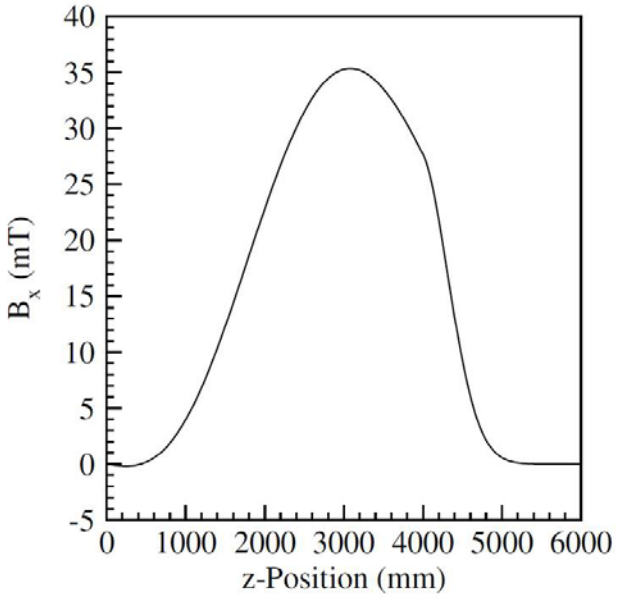

Figure A3: Anti-DID field strength for LDC, as used in A. Vogel's thesis (copied from Figure B4 of [A9]).

Studies of the vertex detector occupancy for different field configurations have also been performed at around the time of the ILD LoI (see [A10] and [A11]), but no details on the shape and strength of the anti-DID field can be found in these papers.

A more recent thesis by R. Versteegen [A12], partially published in [A13], is concerned with beam optics and trajectory corrections for ILC in the presence of detector solenoid, anti-solenoid and anti-DID fields. Both cases, SiD and ILD, are treated. In this work, the anti-DID field assumed for ILD has a different shape and peak value compared to the one in [A6] and [A9] (cf. Figure A1). While this thesis gives [A5] as a reference concerning the evolution of DID and anti-DID at ILC, there is no reason or reference given for the very different anti-DID field shape used. However, recently R. Versteegen [A14]

explained the origin of the anti-DID field used in [A12]: The original design of B. Parker (cf. Figure A2) was used and adapted to ILD by O. Delferrière, see [A15]. Since the field in [A15] seemed a bit too strong for the 14 mrad crossing angle of ILC, R. Versteegen scaled the amplitudes of the anti-DID field – in order to have the field lines aligned to the beam extraction line up to the first quadrupole. The field obtained in this way is the one shown in the thesis [A12].

In a presentation to the ILD workshop 2012 at Kyushu University, Japan, A. Miyamoto presented background studies for ILD [A16]. He introduced the two possible field configurations (labelled "sub_detector" in Mokka), i.e. ***fieldX02*** and ***fieldX03***. According to information provided by A. Sailer [A17], ***fieldX02*** corresponds to the magnetic fields as used for the LCD background studies (i.e. as in A. Vogel's thesis [A9], with ***fieldvalue*** set to 1.0) – the field as implemented in Mokka in June 2012 is shown in Figure A4. On the other hand (again according to A. Sailer [A17]), ***fieldX03*** uses a 2D solenoid field map and the same anti-DID field shape as *fieldX02*, but with ***fieldvalue*** set to 1.1.

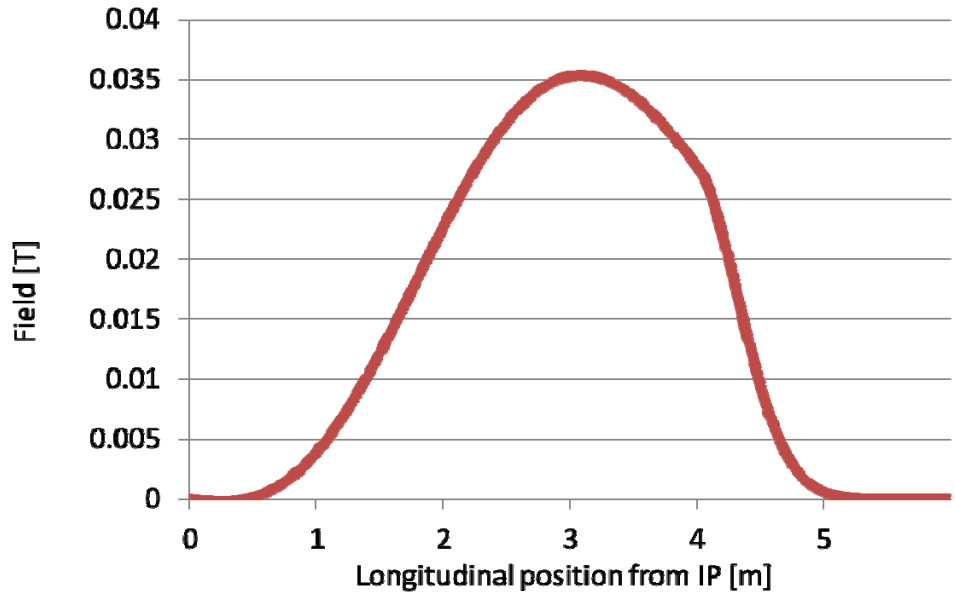

Figure A4: Anti-DID field strength B_x as used for ILD simulations. Values shown are as implemented in Mokka in June 2012 (information provided by A. Sailer [A17]).

The ***fieldX03*** was created by F. Gaede [A18], originally to correct for a deficiency found with ***fieldX02***. In fact, the latter is found unphysical at larger radii, i.e. farther away from the beam pipe. This is not a problem when looking at background hits in the central region (e.g. the vertex detector), but was found to be relevant when studying pair background in the TPC. Therefore, F. Gaede created ***fieldX03*** starting from a 2D field map, and following A. Vogel's procedure of adjusting the anti-DID strength such that low-p_T particles from the IP would follow the field lines into the outgoing beam pipe.

Most recently, and in the final stages of writing the DBD of ILD, further background studies (vertex detector hits) were performed at DESY by E. Avetisyan et al. [A19]. Again, the two field configurations ***fieldX02*** and ***fieldX03*** were used in the simulations. Figure A5 shows the anti-DID field for the two cases. It appears that the peak value is either slightly lower, or slightly higher, when compared with the values shown in [A8] or extracted from Mokka in June 2012 [A17]. The field crosses zero at z = 5 m, as in Fig. [A5]. A slight "undershoot" beyond z = 5 m seems to be a new feature, although this may not be significant due to the low field strength.
A comparison of the two configurations, considering background hits in the ILD vertex detector layers, was made and is given in [A19]. Clearly, the configuration ***fieldX02*** is favoured and was therefore used for the studies in the DBD of ILD.

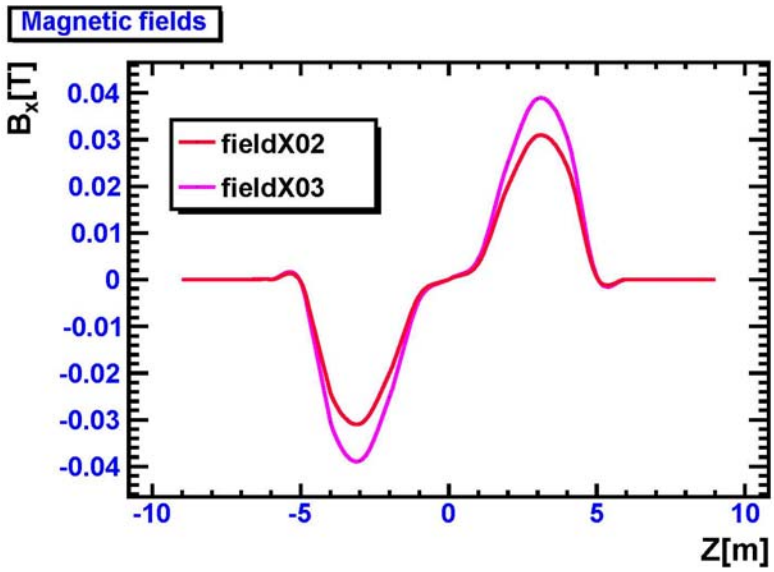

Figure A5: Anti-DID field strength for ILD, as used for DBD studies, for the two MOKKA field configurations ***fieldX02*** and ***fieldX03*** as used in background studies for the ILD DBD (plot courtesy of E. Avetysian, 21 March 2013)

In summary, for the conceptual design of the ILD magnet system described in the DBD, a specification for the anti-DID was needed in summer 2012. Looking at all the options discussed over the years, it was decided at that time to use an anti-DID field shape and magnitude as the one in A. Vogel's thesis [A9] – identical to the one in Mokka in June 2012 (Fig. A4) - for the ILD magnet system design (described in this LC note). During the course of the detailed design studies including full 3D magnet calculations, however, it turned out that it is difficult to produce a field exactly of the shape as given in Fig. A4. Further iterations between the magnet designers and the physics/background simulations will be needed to conclude on a technically feasible and background-wise acceptable anti-DID field shape.

References in Annex A

[A1] B. Parker and A. Seryi, *Compensation of the effects of a detector solenoid on the vertical beam orbit in a linear collider,* PRSTAB **8**, 041001 (2005)

[A2] T. Behnke et al., *ILC Reference Design Report Volume 4 – Detectors*, (2007) arXiv:0712.2356

[A3] The ILD Concept Group, *The International Large Detector: Letter of Intent,* (2009) arXiv:1006.3396

[A4] H.Aihira et al., *SiD Letter of Intent*, (2009) arXiv:0911.0006

[A5] A. Seryi, T. Maruyama and B. Parker, *IR Optimization, DID and anti-DID,* SLAC-PUB-11662 (contributed paper to the 36th ICFA Advanced Beam Dynamics Workshop NANOBEAM 2005)

[A6] A. Seryi, Web Page of the SLAC Beam Delivery Meeting on 2005-10-04, October 2005, http://www-project.slac.stanford.edu/lc/bdir/Meetings/beamdelivery/2005-10-04/index.htm

[A7] R. Settles and W. Wiedenmann, *The Linear Collider TPC: Revised Magnetic-field Requirements,* LCD-Note-2008-001

[A8] D. Toprek and Y. Nosochkov, *Evaluation and Compensation of Detector Solenoid Effects on Disrupted Beam in the ILC 14 mrad Extraction Line,* SLAC-PUB-13492 (2008)

[A9] A. Vogel, *Beam Induced Backgrounds in Detectors at the ILC,* PhD Thesis, University of Hamburg, August 2008, and private communication, 3 April 2013

[A10] A. Besson et al., *Estimation of the background on the vertex detector of ILD from beamstrahlung,* ILC Note 2008 (31 March 2009)

[A11] R. De Masi and M. Winter, *Improved Estimate of the Occupancy by Beamstrahlung Electrons in the ILD Vertex Detector,* arXiv:0902.2707

[A12] R. Versteegen, Conception et Optimisation de la Région d'Interaction d'un Collisionneur Linéaire Electron-Positon, PhD Thesis, Université Paris-Sud 11 (2011)

[A13] R. Versteegen et al., *Optics Studies for the Interaction Region of the International Linear Collider,* paper WEPE001, Proceedings of IPAC'10, Kyoto, Japan (2010)

[A14] R. Versteegen, private communication, 20 February 2013 and 27 March 2013

[A15] O. Delferrière, *Magnetic System Overview- Solenoid and DID,* presentation to the ILD workshop held in Paris, January 2010, see slides at http://ilcagenda.linearcollider.org/getFile.py/access?contribId=7&sessionId=2&resId=1&materialId=slides&confId=4332

[A16] A. Miyamoto, *A study of pair backgrounds - Preliminary study of pair background hits with new ILD detector models and updates since KILC12,* presented at the ILD workshop in Fukuoka, Japan, May 2012, see slides at http://ilcagenda.linearcollider.org/getFile.py/access?contribId=41&sessionId=3&resId=1&materialId=slides&confId=5496

[A17] A. Sailer, private communication, 20 June 2012 and 24 January 2013.

[A18] F. Gaede, private communication, 27 March 2013

[A19] E. Avetisyan, *Update on Pair Background Studies*, presentation given to the ILD analysis meeting of 23 January 2013, see slides at http://ilcagenda.linearcollider.org/getFile.py/access?contribId=1&resId=0&materialId=slides&confId=5959 and *Study of the anti-DID Magnetic Fields' Effects on the Beam-induced Pair Backgrounds in ILD,* LC-REP-2013-002, in preparation